sEMG-Based Identification of Hand Motion Commands Using Wavelet Neural Network Combined With Discrete Wavelet Transform

Feng Duan, Lili Dai, Wennan Chang, Zengqiang Chen, Chi Zhu, *Member, IEEE*, and Wei Li, *Member, IEEE*

***Abstract*—Surface electromyogram (sEMG) signals can be applied in medical, rehabilitation, robotic, and industrial fields. As a typical application, a myoelectric prosthetic hand is controlled by the sEMG signals of the amputee's residual muscles. To improve the dexterity of the myoelectric prosthetic hand, additional hand motion commands need to be classified. The more sEMG sensors are used, the more hand motion commands can be classified. However, the amputee's residual muscles are limited. In order to improve the practicability of the myoelectric prosthetic hand, it is critical to investigate the effective pattern recognition algorithms to deal with the sEMG signals detected by fewer sensors, while identifying as many hand motion commands as possible. Current pattern recognition algorithms for sEMG signals are challenged by limited recognition patterns and unsteady classification accuracy rates. To solve these dilemmas, we employed discrete wavelet transform (DWT) and wavelet neural network (WNN) algorithms to improve the pattern recognition effects of sEMG signals. In addition, the back propagation and gradient descent algorithms were utilized to train WNN. In this work, we only used three sEMG sensors to classify and recognize six kinds of hand motion commands. The maximum identification accuracy rate is 100%, and an average classification accuracy rate of the proposed WNN is 94.67%, which is substantially better than the artificial neural network (ANN) algorithm.**

***Index Terms*—Discrete wavelet transform (DWT), prosthetic hand, surface electromyogram (sEMG) signal, time-frequency domain, wavelet neural network (WNN).**

Manuscript received March 26, 2015; revised July 12, 2015; accepted September 9, 2015. Date of publication November 2, 2015; date of current version February 8, 2016. This work was supported in part by the National Natural Science Foundation of China under Grant 61203339, in part by the Doctoral Fund of the Ministry of Education of China under Grant 20110031120041, in part by the Key Technologies R&D Program of Tianjin under Grant 14ZCZDSY00008 and Grant 14RCGFGX00848, in part by the Tianjin Research Program of Application Foundation and Advanced Technology under Grant 14JCYBJC18300, and in part by the Scientific Research Foundation for Returned Overseas Chinese Scholars, State Education Ministry, under Grant [2012] 940 *(Corresponding authors: Feng Duan and Chi Zhu.)*

F. Duan, L. Dai, W. Chang, and Z. Chen are with the Department of Automation and Intelligence Science, College of Computer and Control Engineering, Nankai University, Tianjin 300071, China (e-mail: duanf@nankai.edu.cn).

C. Zhu is with the Department of Systems Life Engineering, Maebashi Institute of Technology, Maebashi 371-0816, Japan (e-mail: zhu@maebashi-it.ac.jp).

W. Li is with California State University, Bakersfield, CA 93311 USA, and also with Tianjin University, Tianjin 300072, China.

Digital Object Identifier 10.1109/TIE.2015.2497212

I. Introduction

MYOELECTRIC control is an advanced technique to control human-support robots, industrial electronic equipment, or rehabilitation devices, such as surface electromyogram (sEMG)-based wheelchair controller [1], [2], exoskeletons [3], [4], industrial robots [5], diagnoses, and clinical applications [6], [7]. These applications mainly focus on normal people; however, the amputees have strong demands to improve their quality of life (QOL). Moreover, a myoelectric prosthetic hand that works according to human intention brings great benefits to amputees. Thus, this paper intends to investigate the sEMG-based identification of hand motion commands for the myoelectric prosthetic hand. The myoelectric prosthetic hand is controlled by the sEMG signals of the amputee's residual muscles. Most of the current commercially available myoelectric prosthetic hands, such as OttoBock SensorHandTM [8], Motion Control Hand [9], Bebionic3 Hand [10], and iLimb Hand [11], can generate limited human-like grasping and manipulation motions. However, the myoelectric control systems of these products are controlled by the switch ON–OFF commands in single muscle groups, and only limited hand motion commands can be classified. This is important because the more hand motion commands can be classified, the more dexterity of the myoelectric prosthetic hand can be obtained to improve the QOL of the amputees.

Hence, previous researchers have focused on developing and optimizing the sEMG pattern recognition system to classify as many hand motion commands as possible. Hori [1] analyzed one channel of sEMG signals to obtain the power-assisted command. Alkan [12] detected two channels of sEMG signals from biceps brachii and triceps brachii, and classified four hand motion commands. Khezri [13] and Englehart [14] utilized four channels and classified six hand motion commands. Xing [15] classified seven hand movements based on four sEMG sensors. Phinyomark [16] acquired sEMG signals of five channels and classified six hand motions. In order to classify 10 hand motion commands, Rafiee [17] recorded the sEMG signals from 16 locations on the forearm, whereas Karimi [18] used 22 sEMG sensors. These studies focused on designing an effective sEMG pattern recognition system to classify more complex hand motion commands with higher accuracy, but did not pay close attention to limiting the number of sEMG sensors. Although increasing the number of sEMG sensors may contribute to the classification effects of hand motion commands,

it increases the complexity of classification algorithms and deteriorates the real-time performance of the sEMG pattern recognition system. In addition, it is impractical to fix more than three sEMG sensors inside of the fixed cavity of a prosthetic hand due to the amputee's limited residual muscles. To balance the dilemma between the dexterity of the prosthetic hand and the limited sEMG sensors, this paper aims to propose an sEMG pattern recognition system that utilizes three sEMG sensors to identify six hand motion commands.

Generally, an sEMG signal pattern recognition system consists of a feature extraction part and a classification part. Time domain analysis, frequency domain analysis, and time-frequency domain analysis constitute the main methods during the feature extraction process. Since the sEMG signals are recorded in the time domain, time domain analysis is one of the popular methods to extract the sEMG features. Previous studies utilized root mean square (RMS) [19], mean absolute value (MAV) [20], autoregressive (AR) [21], and others to extract the sEMG features. Khushaba [22] extracted sEMG features from the time domain to form a set of features invariant to limb position. sEMG signals also contain various frequency components, which can be analyzed by frequency domain analysis methods [23]. Furthermore, time-frequency domain analysis methods can integrate the advantages of both time domain and frequency domain analysis methods. Wavelet transform (WT) is one of the time-frequency analysis methods, and it is viewed as an alternative to the usual Fourier transform method [24]. WT can be divided into a discrete form and a continuous form. Kexin [15] employed the wavelet packet transform (WPT) method to extract time and frequency information. Discrete WT (DWT) can decompose sEMG signals into orthonormal time series with different frequency bands [25], [26].

In addition to the feature extraction part, an appropriate classifier determines the number and the accuracy of the classified hand motion commands. Researchers have investigated the effects of a series of classification methods, including Bayesian techniques [27]–[31], neural networks [32]–[36], multilayer perceptron [37], [38], fuzzy approaches [39]–[41], support vector machines [42]–[45], and neuro-fuzzy systems [13], [46]–[48]. Due to the nonlinearization and stochasticity of the sEMG signals, the classifier with nonlinear model can improve the classification accuracy of hand motion commands. Neural network, as a nonlinear statistical data modeling tool, plays an important role in sEMG classification and yields high-accuracy results [49]. The back propagation neural network is good at training self-learning feed-forward neural networks, which is commonly used to classify sEMG patterns. However, back propagation neural network requires a large quantity of training data and requires too many learning iterations [50]. On the contrary, wavelet neural network (WNN) was found to constitute an ideal technique to classify the sEMG patterns, since WNN combines the advantages of the wavelets' time-frequency domain characteristics and the ANN's learning ability [51].

Considering the advantages identified by previous studies, we proposed a novel sEMG pattern recognition system in this paper. In this sEMG pattern recognition system, DWT is utilized to decompose the sEMG signals detected by three channels and extract the sEMG features in the time-frequency domain; WNN is employed to classify six hand motion commands. In addition, artificial neural network (ANN) is used as a counterpoint to evaluate the WNN's classification effect.

This paper is organized as follows. Section II describes the sEMG signals acquisition. Section III briefly introduces the basic principle of the WT method, and explains the sEMG feature extraction process by DWT. Section IV explains the construction of the WNN classifier. Section V shows the experimental results, and compares the classification effect of the proposed method with that of the conventional ANN method. Finally, conclusion and future work are given in Section VI.

II. sEMG Acquisition

The electromyogram (EMG) signal is a bioelectrical signal variation generated during the muscle contraction process. The EMG signal is a complicated biomedical signal influenced by anatomical or physiological properties of the muscles and the environmental noises [12]. Thereby, the collection of EMG signal is a fundamental task that influences the next identification of hand motion commands. Generally, EMG signals can be detected by invasive or noninvasive electrodes. The EMG signals collected by invasive needles or wire electrodes are suitable to investigate deep muscle structure. However, due to their noninvasiveness and convenient operation, sEMG techniques are mainly used to detect sEMG signals in the fields of biofeedback, prosthetic hand control, movement analysis, etc. Hence, we used sEMG as original signals to control the prosthetic hand.

Since we aim to recognize more hand motion commands only based on three sEMG sensors, the sensor position is crucial to the identification accuracy. Considering the kinematic physiological characteristics of human hand and the corresponding forearm muscles, we chose four commonly used hand motions at first, namely hand closing (HC), hand opening (HO), wrist extension (WE), and wrist flexion (WF).

Then, we need to determine the corresponding forearm muscles. Although there are deep layer and superficial layer muscles that contribute to the above hand motions, the sEMG signals are mainly influenced by the superficial layer muscles. Therefore, we selected three superficial layer muscles to fix the sEMG sensors (refer to Fig. 1). Extensor carpi radialis longus, which is on the posterior side of the forearm, acts to extend and abduct the hand at the wrist. Flexor carpi radialis assists in the wrist flexion and the wrist abduction. Extensor digitorum acts to extend the phalanges and the wrist, and it tends to separate the fingers as it extends the phalanges. In this paper, the sEMG sensors were placed on the extensor carpi radialis longus (CH.A), the flexor carpi radialis (CH.B), and the extensor digitorum (CH.C) of the subject's forearm, respectively (refer to Fig. 1).

The acquired sEMG signal is the superimposition of EMG signals from the muscles below and around the sEMG sensor. The extensor carpi radialis longus is in the upper level of the supinator, and the flexor carpi radialis is near the pronator teres. Moreover, supinator and pronator teres serve to forearm supination (FS) and forearm pronation (FP), respectively. Consequently, we can choose FP and FS as two additional

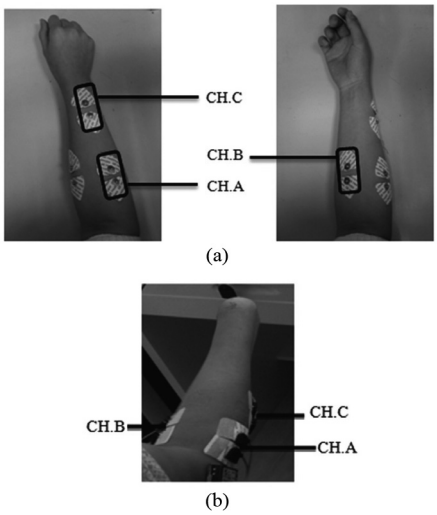

Fig. 1. Position of sEMG sensors. Channel A is placed on the extensor carpi radialis longus; Channel B is placed on the flexor carpi radialis; and Channel C is placed on the extensor digitorum. (a) Position of sEMG sensors of a healthy subject. (b) Position of sEMG sensors of an amputee.

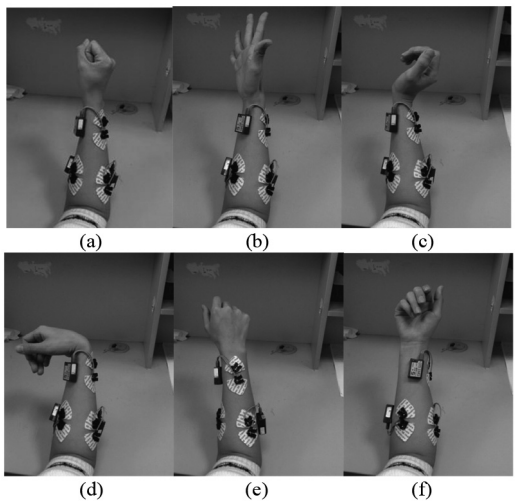

Fig. 2. Six classes of hand movements utilized in this paper. (a) HC. (b) HO. (c) WE. (d) WF. (e) FP. (f) FS.

hand motions without increasing the number of sEMG sensors. Totally, six hand motions can be classified by three sEMG sensors, namely HC, HO, WE, WF, FP, and FS (as shown in Fig. 2).

In order to classify more hand motions with fewer sEMG sensors, the sensor position is crucial to the identification accuracy. Therefore, we calculated RMS of sEMG signals acquired from CH. A to CH. C. As illustrated in Fig. 3, the calculated RMS values of sEMG signals detected from CH. A, CH. B, and CH. C are listed from top to bottom in turn. The identified hand motions, such as HC, HO, WE, WF, FP, and FS are listed from left to right. Each hand motion continues about 5 s, and the interval between two adjacent hand motions is about 10 s. According to Fig. 3, when the subject executes different hand motions, the RMS values of three sensors are different. For example, when the HO is executed, the RMS value of CH. C is the largest among three sensors. In the case of WE, the

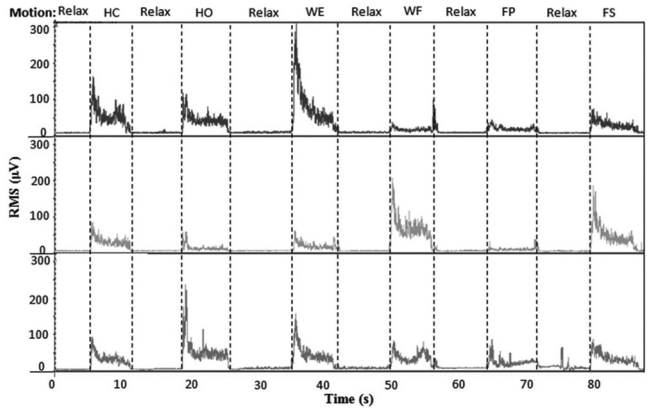

Fig. 3. RMS values of sEMG signals from three sensors.

RMS value of CH. A changes greatly. While in the case of WF, the RMS value of CH. B is more than that of the other two sensors. According to the obvious changes of RMS values, it can be concluded that the determined sensor positions contribute to the identification of the selected six hand motions.

To reduce the influence of skin (e.g., impedance, superficial oil content, and dead cell layer), we wiped the skin of desired locations on the forearm with alcohol. Moreover, two channels of differential surface Ag–AgCl electrodes with 20 mm interelectrode distance were utilized to collect sEMG signals after the skin dried. The sEMG signals were recorded with a sampled rate of 1500 Hz using TeleMyob2400 G2 (Noraxon, USA).

Six healthy subjects participated in the experiment, namely four women who were 23, 23, 25, and 26 years old, and two men who were 23 and 36 years old, respectively. Some rehabilitation experts have suggested that one should use healthy subjects for initial evaluation objectives [14], [40]. Thereby, the sEMG of healthy subjects is an appropriate emulation of the amputee's sEMG. To further demonstrate the practicability and the validity of the proposed identification method, two amputees were required to execute the same experiment (refer to Fig. 1).

All of the subjects performed above six hand movements. For each subject, we selected 100 sEMG signals of one hand movement. Since there are six hand movements that need to be classified, a total of 600 sEMG signals were collected for each subject. In order to control the prosthetic hand in real time, the response time should be less than 300 ms. Therefore, 200 ms was selected as the appropriate time window length of the sEMG signal [13]. There are 300 points for one signal. Since sEMG signals are different from one subject to another, we divided the acquired sEMG signals into two sets for each subject. One is the training set, the other is the test set, and each set has 300 sEMG signals.

III. sEMG Feature Extraction Using WT

After collecting sEMG signals, we need to extract the feature vectors of sEMG signals. Taking the advantages of both time domain analysis and frequency domain analysis, the WT, as a time-frequency domain analysis, was utilized in this paper.

A. Wavelet Transform

A wavelet $\psi_{a,b}(t)$ is derived from its mother wavelet $\psi(\cdot)$ by dilating and time-shifting. This relation can be defined as

$$\psi_{a,b}(t) = \frac{1}{\sqrt{|a|}}\psi\left(\frac{t-b}{a}\right) \tag{1}$$

where a and b represent the scaling factor and the translation factor, respectively. The family of functions generated by $\psi(\cdot)$ can be defined as

$$\Omega = \{\psi_{a,b}(t), a \in \Re, b \in \Re, a \neq 0\}. \tag{2}$$

Ω is called a frame of $L^2(\Re)$ if it satisfies the admissibility condition C_ψ

$$C_\psi = \int_0^{+\infty} \frac{|\psi(\omega)|^2}{\omega} d\omega < +\infty \tag{3}$$

where $\psi(\omega)$ is generated from $\psi(t)$ by Fourier transform. There is a function $f(t) \in L^2(\Re)$, and its continuous WT is defined as the inner product of functions $f(t)$ and $\psi_{a,b}(t)$

$$\begin{aligned} \mathrm{CWT}(a,b) &= \langle f(t), \psi_{a,b}(t)\rangle \\ &= \frac{1}{\sqrt{a}}\int_{-\infty}^{+\infty} \psi^*\left(\frac{t-b}{a}\right) f(t)dt, \quad a > 0 \end{aligned} \tag{4}$$

where $\psi^*\left(\frac{t-b}{a}\right)$ is the conjugate function of $\psi\left(\frac{t-b}{a}\right)$.

The discrete version of WT of a discrete signal $f(n)$ is defined as

$$\mathrm{DWT}(j,k) = \frac{1}{\sqrt{{a_0}^j}} \sum_n \psi\left(\frac{n - kb_0{a_0}^j}{{a_0}^j}\right) f(n), \quad a_0 > 0 \tag{5}$$

where $a = {a_0}^j, b = kb_0{a_0}^j$; j, k, and n are integers; and j is the depth of decomposition [52]. The time-frequency analysis based on the DWT is well suited to nonstationary signals whose frequency spectrum is time-variant. Some approaches have appeared in the literature that used DWT in handling EMG [52], [53]. Compared with Hudgins' time domain approach, a wavelet-based approach exhibits superior performance [14]. To avoid complicated computations, in (5), we set $a_0 = 2$ and $b_0 = 1$. Then, we have a dyadic sampling in time axes, and the following dyadic wavelet can be obtained:

$$\psi_{j,k}(t) = \frac{1}{\sqrt{2^j}}\psi\left(\frac{n}{2^j} - k\right) \tag{6}$$

where j, k, and n are integers.

For most signals, the analytical solution cannot be resolved by DWT, so it can only be obtained by numerical algorithm. Therefore, it requires a fast calculation method to make DWT be applied in practice. Mallat proposed MALLAT algorithm to realize the multiresolution signal decomposition rapidly [54], [55], which is an important part in WT. Hence, we used the MALLAT algorithm (described in Fig. 4) for DWT to process sEMG signals. The original signal A_0 is decomposed into approximations A_{-1} and details D_{-1}, then A_{-1} is

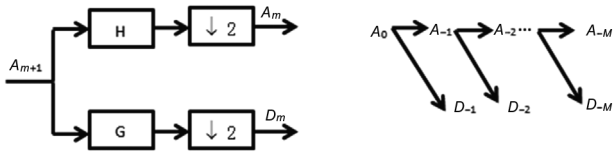

Fig. 4. MALLAT algorithm. Note that "A_0" is the original signal, and "↓ 2" is keeping one sample out of two.

decomposed into approximations A_{-2} and details D_{-2}, and so on, until a predetermined level. This relationship can be expressed as

$$A_m(n) = \sum_k h(2n-k)A_{m+1}(k) \tag{7}$$

$$D_m(n) = \sum_k g(2n-k)A_{m+1}(k) \tag{8}$$

where $m = -1, -2, \ldots, -M$. In Fig. 4, G is the high-pass filter, and H is the low-pass filter. The impulse response $g(k)$ of filter G is related to the impulse response $h(k)$ of the filter H [54]

$$g(k) = (-1)^{1-k}h(1-k). \tag{9}$$

B. Features Selection

The approximate part mainly consists of low-frequency signals; whereas the details mainly consist of high-frequency signals. The value of coefficients represents the fitting extent of the signals, and higher values indicating greater similarity. Therefore, we can choose the maximum absolute value of the coefficients as the feature vector of sEMG signals. One method is to select the maximum absolute value of approximate coefficients of every level, marked as AAA; the other method is to choose the maximum absolute value of approximate coefficients of the last level and the maximum absolute value of detail coefficients of every level, marked as ADDD. The decomposition level is represented by n. Because the sEMG signals were detected from three sensors, there is a $3n$-dimensional feature vector of AAA and a $3(n+1)$-dimensional feature vector of ADDD. Considering the computational complexity, we cannot decompose sEMG signals into many levels. Hence, the obtained sEMG signals were decomposed by DWT level-3 decomposition. For example, the level-3 decomposition process of sEMG signals detected from CH.C is illustrated in Fig. 5. The feature vector selection influences the classification results significantly [16], and the suitable feature vector should be selected by using DWT to deal with sEMG signals. Therefore, the contrast experiment was done to choose the better feature vector from AAA and ADDD. In this experiment, we collected three healthy subjects' sEMG signals. Each subject performed the proposed six hand movements, and the results are shown in Fig. 6. All three subjects' average classification accuracy rates of ADDD are above 90%, and the average classification accuracy rate of ADDD is much higher than that of AAA. Consequently, a 12-dimensional feature vector of ADDD was selected as the input of the WNN.

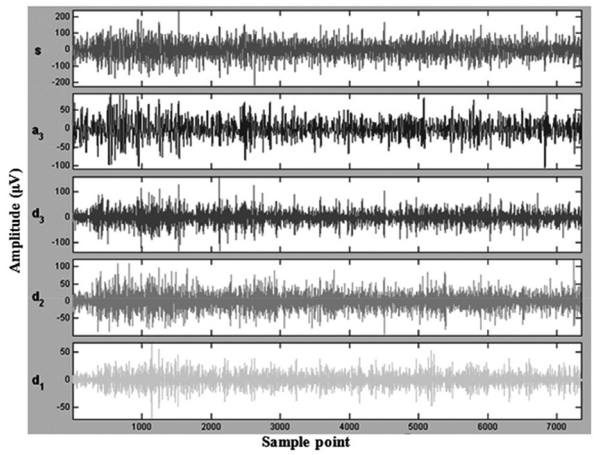

Fig. 5. Decomposed sEMG signal by DWT level-3 decomposition from CH.C. Note that "s" is the original signal. "a_3" is the approximation at the third level. "d_3" is the details at the third level. "d_2" is the details at the second level. "d_1" is the details at the first level.

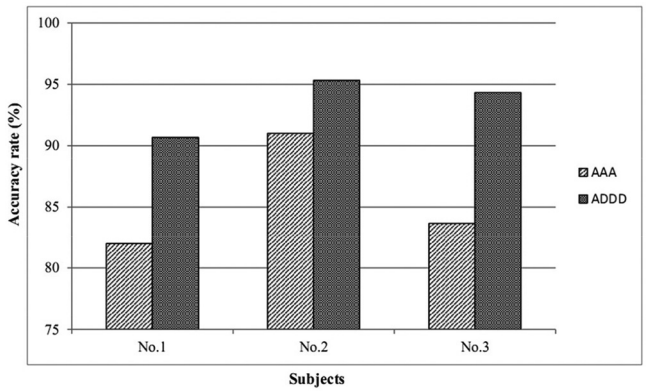

Fig. 6. Feature selection results.

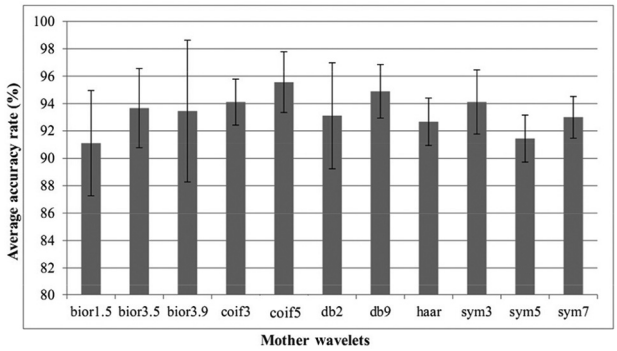

Fig. 7. Average accuracy rate of mother wavelet selection. Note that "bior1.5", "bior3.5", and "bior3.9" belong to biorthogonal wavelets; "coif3" and "coif5" belong to coiflet wavelets; "db2" and "db9" belong to Daubechies wavelets; "haar" is a Haar wavelet; "sym3", "sym5", and "sym7" belong to symlet wavelets.

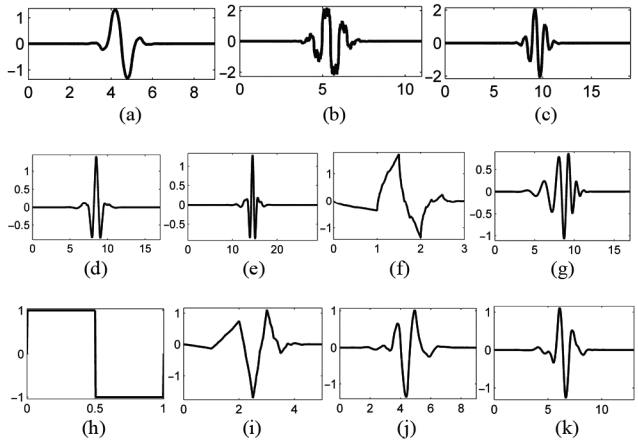

Fig. 8. Mother wavelets. (a) bior1.5. (b) bior3.5. (c) bior3.9. (d) coif3. (e) coif5. (f) db2. (g) db9. (h) haar. (i) sym3. (j) sym5. (k) sym7.

C. Best Mother Wavelet Selection

Different wavelet functions have different time-frequency characteristics and affect the performance of WT, so it is important to select an appropriate wavelet function for the wavelet analysis. To construct a feature set through DWT, we need to determine the type of mother wavelet. On the basis of the feature selection results, we used the feature vector of ADDD to investigate the classification accuracy rates of eleven different dominant mother wavelets, such as Haar, biorthogonal, coiflet, Daubechies, and symlet with different orders. Above five types of mother wavelets, all have biorthogonality and compact support, and they are commonly used in DWT. In the feature extraction part, the feature should contain enough information to maintain the classification accuracy of the hand motion commands. Hence, we determined the best mother wavelet according to the classification accuracy rate. In this paper, eleven different mother wavelets are marked as "bior1.5," "bior3.5," "bior3.9," "coif3," "coif5," "db2," "db9," "haar," "sym3," "sym5," and "sym7". Fig. 7 depicts the average accuracy rates of three subjects and the standard deviation of each type of mother wavelet. In Fig. 7, "coif5," with the maximum classification accuracy rate and smaller standard deviation, is selected as the best mother wavelet for sEMG feature extraction. In this paper, we chose the wavelet coefficients as feature vector of sEMG signals, and the wavelet coefficients reflect the degree of similarity between the wavelet function and the decomposed sEMG signals. The larger the wavelet coefficient is, the higher the degree of similarity is. Thus, choosing the mother wavelet with higher degree of similarity is beneficial to the analysis of sEMG signals. The original sEMG signals (refer to Fig. 5) are nonstationary and nondecaying, so the mother wavelets with decay (as "bior3.9," "db9," "sym7") are not appropriate, according to the mother wavelets' waveforms in Fig. 8. Moreover, the Haar wavelet is discontinuous in time domain, so it is also not appropriate. The coiflet wavelets' waveforms are similar to the sEMG signals, so the average accuracy rate of six hand motions using "coif5" is high.

The coiflet wavelet with L orders is the compactly supported orthogonal wavelet, which satisfies the following two vanishing moment conditions in (10) and (11) [56]. Equation (10) means that the vanishing moment of the scaling function $\phi(t)$ equals to 0. Equation (11) means that the vanishing moment of the mother wavelet $\psi(t)$ equals to 0

$$\int t^l \phi(t)dt = \begin{cases} 1, & l = 0 \\ 0, & l = 1, 2, \ldots, L-1 \end{cases} \tag{10}$$

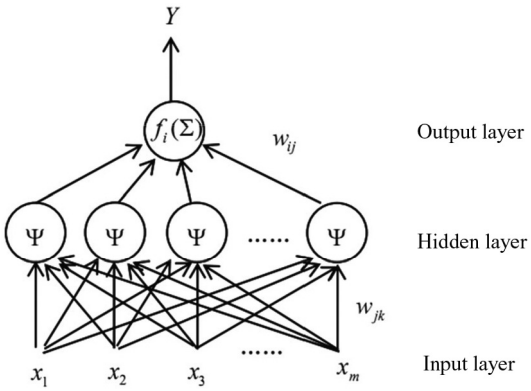

Fig. 9. Structure of WNN.

$$\int t^l \psi(t) dt = 0, \quad l = 0, 1, \ldots, L-1. \tag{11}$$

The mother wavelet "coif L" has $2L$ vanishing moments that equal to 0 and a support of length $6L-1$. For a given support width, the mother wavelet "coif L" is a compactly supported wavelet with the highest number of vanishing moments for both mother wavelet (psi) and scaling function (phi) [57]. In this paper, L is set as 5.

IV. Classification Using WNN

The classifier is the most significant part that influences the identification accuracy of the hand motion commands. Among various classification algorithms, WNN offers special advantages [58], [59]. In this paper, we utilized WNN to accomplish pattern recognition. The structure of WNN is shown in Fig. 9. It consists of three layers, which are the input layer, the hidden layer, and the output layer.

The m-dimensional feature vector as the input of WNN in Fig. 9 is defined as $\boldsymbol{X}$

$$X = [x_1 \quad x_2 \quad \ldots \quad x_m]. \tag{12}$$

The N-dimensional vector as the output of WNN in Fig. 9 is defined as $\boldsymbol{Y}$

$$Y = [y_1 \quad y_2 \quad \ldots \quad y_N]. \tag{13}$$

These 12 feature extraction coefficients are used as inputs to WNN, so $m = 12$. We determined the number of hidden layer nodes as 25, by using the empirical formula

$$p = 2m + 1 \tag{14}$$

where p denotes the number of hidden layer nodes. In order to identify six hand movements, the number of output layer nodes is set as six, in other words, $N = 6$. We defined six different unit vectors, which are called class labels, to represent six hand movements. The weight w_{jk} in Fig. 9 means the correlation between x_k of the input layer and the jth node of the hidden layer. The weight w_{ij} in Fig. 9 means the correlation between the jth node of the hidden layer and y_i of the output layer. The larger the value of weight, the stronger the correlation between two adjacent layers. The input of the jth node of hidden layer is expressed as follows:

$$\text{net}_j = \sum_{k=1}^{m} w_{jk} x_k, j = 1, 2, \ldots, p. \tag{15}$$

The output of the jth node of the hidden layer related to the mother wavelet activation function is defined as

$$\Psi_{(a_j, b_j)}(\text{net}_j) = \Psi\left(\frac{\text{net}_j - b_j}{a_j}\right), \quad j = 1, 2, \ldots, p \tag{16}$$

where a_j and b_j represent the scaling factor and the translation factor, respectively. If $a_j > 1$, it means that the function is tensile. If $0 < a_j < 1$, it indicates that the function is compressed. WNN requires the above two functions, thereby, the initial value of a_j is in the range of 0 to 5. As far as the parameters of a_j are concerned, one part has compression ability and the other part has tension ability. Scaling factor b_j is mapped to the range from -10 to 10. The final output y_i is expressed as follows:

$$y_i = \sum_{j=1}^{p} w_{ij} \Psi_{(a_j, b_j)}(\text{net}_j), \quad i = 1, 2, \ldots, N. \tag{17}$$

The desired output of the ith node of output layer is d_i. The objective function is defined as

$$E = \frac{1}{2} \sum_{i=1}^{N} (y_i - d_i)^2. \tag{18}$$

The sEMG signals of the training set contain six kinds of class labels, which represent six different hand movements. These sEMG signals were used as the input to train the WNN. If the output result and class label are completely consistent, E is equal to 0. In this study, in order to obtain the minimum value of the objective function, the weights, the scaling factor, and the translation factor are updated by the following formulas:

$$\begin{aligned} w_{jk} &= -\eta_1 \frac{\partial E}{\partial w_{jk}} + w_{jk} \\ w_{ij} &= -\eta_1 \frac{\partial E}{\partial w_{ij}} + w_{ij}, \\ & i = 1, 2, \ldots, N; \quad j = 1, 2, \ldots, p; \quad k = 1, 2, \ldots, m \end{aligned} \tag{19}$$

$$\begin{aligned} a_j &= -\eta_2 \frac{\partial E}{\partial a_j} + a_j \\ b_j &= -\eta_2 \frac{\partial E}{\partial b_j} + b_j, \\ & j = 1, 2, \ldots, p \end{aligned} \tag{20}$$

where η_1 and η_2 are learning rates.

As described in (19) and (20), the iterative procedure with the direction of a descent makes the objective function arrive at its minimum value. At the same time, the iterative procedure with the back propagation makes the weights, the scaling factor, and the translation factor arrive at appropriate values. Finally, we determined the best parameters of WNN by the gradient descent method and the back propagation.

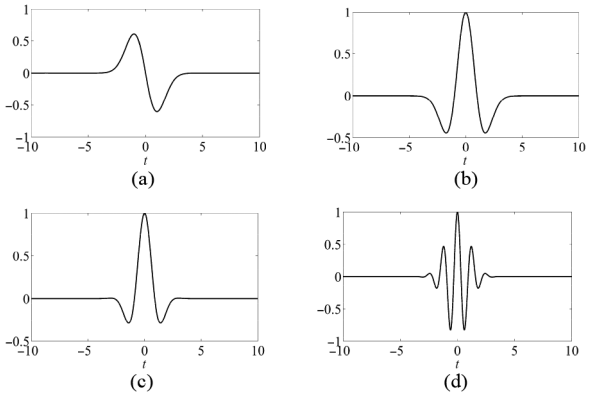

Fig. 10. Four types of mother wavelets. (a) Gaussian wavelet. (b) Mexican Hat wavelet. (c) Morlet wavelet I. (d) Morlet wavelet II.

TABLE I
RESULTS OF DIFFERENT MOTHER WAVELET ACTIVATION FUNCTIONS

Subject	Gaussian	Mexican Hat	Morlet I	Morlet II
No. 1	92.67	90.67	93.00	86.33
No. 2	97.33	88.67	97.00	91.33
No. 3	95.33	93.67	97.00	95.00
Average correctness (%)	95.11	91.00	95.67	90.89

The capability of WNN can be affected by various factors, such as the dimension of the input vector, the number of hidden layer nodes, and the mother wavelet activation function. In order to investigate the influence of different mother wavelets on the performance of the proposed WNN, four types of wavelet families [60] were used as the mother wavelet activation functions, respectively. These mother wavelets are Gaussian wavelet, Mexican Hat wavelet, Morlet wavelet I, and Morlet wavelet II (shown in Fig. 10), which are defined as follows:

1) Gaussian wavelet, $\psi_1(t) = -t \cdot \exp(-0.5t^2)$;
2) Mexican Hat wavelet, $\psi_2(t) = (1-t^2) \cdot \exp(-0.5t^2)$;
3) Morlet wavelet I, $\psi_3(t) = \cos(1.75t) \cdot \exp(-0.5t^2)$;
4) Morlet wavelet II, $\psi_4(t) = \cos(5t) \cdot \exp(-0.5t^2)$.

To maintain the consistency of the experiment, three subjects were asked to do the same six hand movements mentioned above. According to the classification results in Table I, the Morlet I wavelet, with the best performance, was chosen as the wavelet function that was used in WNN to classify hand motion commands.

V. EXPERIMENTAL RESULTS AND DISCUSSION

Generally, there are four steps to classify hand movements: 1) acquiring sEMG signals; 2) extracting the feature of each sEMG signal; 3) building a pattern-recognition classifier; and 4) training the pattern-recognition classifier and testing the classification efficiency.

During the sEMG feature extraction process, we used DWT to extract the sEMG features in the time-frequency domain. The feature vector of AAA and the feature vector of ADDD were compared, and the average results of these feature vectors are presented in Fig. 6. According to Fig. 6, the feature of ADDD, with higher average accuracy rate, was adopted. Furthermore, "coif5," with the maximum accuracy rate, is selected as the best mother wavelet for sEMG feature extraction (shown in Fig. 7).

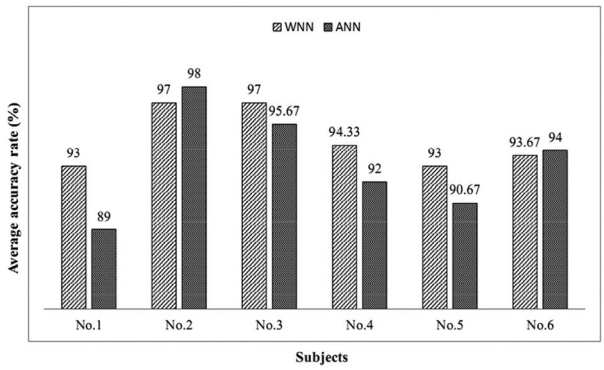

Fig. 11. Classification results of WNN and ANN.

For the construction of the WNN classifier, according to the results in Table I, we selected Morlet I as the best wavelet function for WNN classifying hand motion commands. Furthermore, the gradient descent method and the back propagation method were used to determine the best parameters of WNN.

The number of healthy subjects increased to six for verifying the effectiveness of WNN. Six subjects were required to execute the proposed six hand movements in the same experimental environment. The obtained 600 sEMG signals from each subject were divided into two sets, namely, the training set and the test set. For the convenience of data processing, after collecting the sEMG and extracting the feature vectors, the data in the training set and the test set are standardized by

$$x_{ij}^* = (x_{\max}^* - x_{\min}^*)\frac{x_{ij} - \min\limits_{1\le t\le n}\{x_{tj}\}}{R_j} + x_{\min}^*, \quad i = 1,2,\ldots,n; \quad j = 1,2,\ldots,m \tag{21}$$

$$R_j = \max_{t=1,2,\cdots,n}\{x_{tj}\} - \min_{t=1,2,\cdots,n}\{x_{tj}\}, \quad j = 1,2,\ldots,m. \tag{22}$$

In (21), $x_{\max}^* = 1$, $x_{\min}^* = -1$, and x_{ij} is the jth variable of the feature vector of the ith signal. In (21) and (22), t is an integer, and $m = 12$. "$n = 300$" represents that the amount of the data in both the training set and the test set is 300. After above analysis, we can determine that x_{ij}^* is in the range of -1 to 1.

After training the classifier by the data in the training set, the standardized data in the test set were used as the input of the WNN to verify the classification accuracy. Since ANN is a commonly used method for pattern recognition studies [48], [60], [61], we utilized it to deal with the same standardized data to classify hand motion commands. Fig. 11 shows the results of two different neural networks. The average accuracy rate of WNN is 94.67%, and that of ANN is 93.22%. For all six subjects, all of the accuracy rates of WNN are above 93%; however, the average accuracy rate of ANN varies greatly and the least one is 89%. According to the experimental results, the average accuracy rate of WNN is higher than that of ANN; furthermore,

TABLE II
AVERAGE ACCURACY RATE AND STANDARD DEVIATIONS OF TWO CLASSIFIERS

Classifier	WNN	ANN
Average accuracy rate (%)	94.67	93.22
Standard deviation	1.8736	3.3244

TABLE III
CLASSIFICATION RESULTS OF WNN

Subject	HC	HO	WE	WF	FP	FS
No. 1	90	98	98	100	72	100
No. 2	98	92	98	100	94	100
No. 3	94	100	98	100	92	98
No. 4	96	96	92	88	98	96
No. 5	90	88	86	100	94	100
No. 6	100	84	96	86	96	100
AC (%)	94.67	93.00	94.67	95.67	91.00	99.00

HC, hand closing; HO, hand opening; WE, wrist extension; WF, wrist flexion; FP, forearm pronation; FS, forearm supination; AC, the average accuracy rate.

TABLE IV
CLASSIFICATION RESULTS OF ANN

Subject	HC	HO	WE	WF	FP	FS
No. 1	60	100	100	100	74	100
No. 2	96	94	100	100	100	98
No. 3	88	98	100	98	92	98
No. 4	80	100	88	84	100	100
No. 5	82	86	80	100	98	98
No. 6	100	76	96	94	98	100
AC (%)	84.33	92.33	94.00	96.00	93.67	99.00

HC, hand closing; HO, hand opening; WE, wrist extension; WF, wrist flexion; FP, forearm pronation; FS, forearm supination; AC, the average accuracy rate.

TABLE V
CONFUSION MATRIX FOR GESTURE RECOGNITION BY WNN METHOD

AM	Identified movements					
	HC	HO	WE	WF	FP	FS
HC	94.67	0.67	–	0.33	4.33	–
HO	–	93	–	0.33	3	3.67
WE	0.33	2.33	94.67	–	0.33	2.34
WF	1	–	0.33	95.67	2.67	0.33
FP	2.67	0.33	0.67	0.33	91	5
FS	0.67	0.33	–	–	–	99

AM, actual movements; HC, hand closing; HO, hand opening; WE, wrist extension; WF, wrist flexion; FP, forearm pronation; FS, forearm supination.

TABLE VI
CONFUSION MATRIX FOR GESTURE RECOGNITION BY ANN METHOD

AM	Identified movements					
	HC	HO	WE	WF	FP	FS
HC	84.33	1.67	0.67	0.33	12.33	0.67
HO	–	92.33	0.33	0.33	2.67	4.34
WE	–	0.67	94	–	0.33	5
WF	–	–	–	96	4	–
FP	1	0.33	0.33	0.33	93.67	4.34
FS	–	–	0.33	–	0.67	99

AM, actual movements; HC, hand closing; HO, hand opening; WE, wrist extension; WF, wrist flexion; FP, forearm pronation; FS, forearm supination.

TABLE VII
RESULTS OF WNN RANDOM TEST

Subject	Five random test				
	1	2	3	4	5
No. 1	93.67	92.33	94.33	91.67	94.33
No. 2	99	97	99	98	94.67
No. 3	96.67	97	97	97	96.33
No. 4	94.67	93.33	91.33	91.33	92
No. 5	93.67	96.33	94.33	93.67	94.33
No. 6	96.33	93	97	96.67	94

TABLE VIII
RESULTS OF ANN RANDOM TEST

Subject	Five random test				
	1	2	3	4	5
No. 1	88.33	91.33	91.67	91	94.33
No. 2	98.67	98.33	98.67	98	98.67
No. 3	95	97.33	96	97	94.67
No. 4	88	86	89	89.67	89.33
No. 5	90	92.33	90	83.67	95
No. 6	96	93	96.33	94	96.33

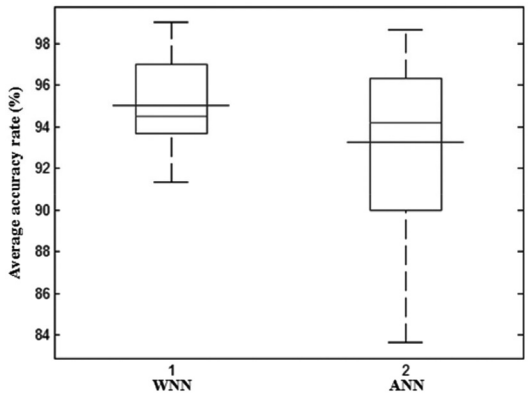

Fig. 12. Box plot of WNN and ANN.

the universal classification results of WNN are better than those of ANN.

Furthermore, the robustness is one of the important parameters that influence the prosthetic hand control performance, so we calculated the standard deviation as an evaluation of the robustness based on the results in Fig. 11. The smaller the standard deviation is, the stronger the robustness is. From Table II, we can know that the robustness of WNN is stronger than that of ANN. In this connection, the capability of WNN is superior to that of ANN.

The classification results of WNN and those of ANN are listed in Tables III and IV, respectively. For the WNN classification method, the lowest average classification accuracy rate of FP is above 91% (refer to Table III); whereas, for the ANN classification method, the average classification accuracy rate of each hand movement varies from 84.33% to 99% (refer to Table IV). This means that the classification stability of WNN is much better than that of ANN.

When an amputee uses a prosthetic hand, the occurrence of wrong actions should be reduced as much as possible. If the sEMG pattern recognition system often misclassifies a hand movement, it is unacceptable for the user. This requires that the sEMG pattern recognition system can classify hand movements

TABLE IX
PERFORMANCE COMPARISON FOR GESTURE RECOGNITION BETWEEN WNN AND ANN

Performance	HC	HO	WE	WF	FP	FS
ME of WNN	4.67	3.66	1	0.99	10.33	11.34
ME of ANN	1	2.67	1.66	0.99	20	14.35
OE of WNN	5.33	7	5.33	4.33	9	1
OE of ANN	15.67	7.67	6	4	6.33	1

ME, misclassification error; OE, omission error; HC, hand closing; HO, hand opening; WE, wrist extension; WF, wrist flexion; FP, forearm pronation; FS, forearm supination.

correctly and stably. For this reason, the pattern recognition method used in this study provides an effective way to identify selected hand movements and control the prosthetic hand.

Confusion matrix, as an effective method in the study of pattern recognition, is used to further verify the true discrimination success of the proposed method. The main purpose of using the confusion matrix is to observe confused or compromised hand movements. If one hand movement is often labeled as another, special pattern recognition efforts must be applied during the actual usage. The confusion matrix that is made up of the average results of all six healthy subjects indicates this confusion problem. Table V depicts the confusion matrix of WNN, and Table VI describes that of ANN, respectively. In this way, the discrimination among the various hand movements of all the subjects can be evaluated completely. In Table V, the lowest classification accuracy rate is 91% (FP). The reason is that the FP classification accuracy rate of the subject no. 1 is lower than that of other five subjects (refer to Table III). However, the average FP classification accuracy rate of other five subjects except the subject no. 1 is 94.8%. The individual difference of the subject no. 1 makes the classification accuracy rate of FP reduced.

The classification accuracy rates listed in Tables V and VI are calculated from 1800 test samples; therefore, the test data used in this paper are large. Hence, the average accuracy rate of WNN (94.67%) is statistically better than that of ANN (93.22%). Furthermore, we did five random tests for each subject to illustrate the superiority of WNN. In these five random tests, we randomly selected 300 samples as the training set, and chose the rest samples as the test set. The contrast average classification accuracy rates between WNN and ANN are shown in Tables VII and VIII. To descript the statistic results graphically, the box plot was drawn in Fig. 12. According to Fig. 12, the accuracy rate of WNN is higher than that of ANN, and the dispersion of WNN is much smaller than that of ANN. Since the data in Tables VII and VIII are paired up, we utilized the paired samples t-test. The null hypothesis was tested by the one-tailed test to judge whether WNN is superior to ANN. The calculated p-value (0.0013) is smaller than the significance level (5%), thus WNN performs significantly better than ANN.

Furthermore, a performance comparison according to the confusion matrix was carried out. The performance obtained by the proposed WNN was compared with the results of ANN. Generally, overall accuracy, misclassification error, and omission error are three factors used to evaluate the confusion matrix. The overall accuracy is defined as the number of diagonal elements per the number of actual hand movements. The overall accuracy of WNN is 94.67%, and that of ANN is 93.22%. The misclassification error is defined as the number of mislabeled classes from one column per the number of actual movements (AM) from the class of the same column. The omission error is defined as the number of mislabeled classes from one row per the number of AM from the class of the same row. The comparison results are shown in Table IX. The misclassification error of FP of ANN and the omission error of HC of ANN are much larger than those of WNN. It means that many samples of HC are mislabeled as other hand motions (shown in Table VI). Moreover, most of the mislabeled HC movements are recognized as the FP movements, so the misclassification error of FP of ANN is large. Even dealing with the same sEMG signals, the misclassification error of FP and the omission error of HC in Table IX are much different. The reason is that WNN has the mother wavelet activation function instead of the sigmoid function [refer to (23)] in ANN. The wavelet activation function $\Psi_{(a_j,b_j)}$ in (16) has the variable scaling factor a_j and the variable translation factor b_j, so WNN has strong adaptability. Compared with WNN, the activation function of ANN in (23) is invariant, so ANN cannot classify the confusing classes effectively. Based on the reasons above mentioned, the performance of WNN and ANN is different in Table IX. Overall, the performance of WNN is more stable than that of ANN

$$f(\text{net}_j) = \frac{1}{1 + e^{-\text{net}_j}}. \tag{23}$$

Furthermore, two upper limb amputees were required to execute the same experiment, and the results are listed in Tables X and XI, respectively. The right arm of subject no. 1 has been amputated below the wrist, and the left arm of subject no. 2 has been amputated below the wrist. The training set contains 300

TABLE X
CLASSIFICATION RESULTS OF AMPUTEES BY WNN

Subject	HC	HO	WE	WF	FP	FS	AC (%)
No. 1	86	70	94	54	78	100	80.33
No. 2	96	76	86	96	88	98	90

HC, hand closing; HO, hand opening; WE, wrist extension; WF, wrist flexion; FP, forearm pronation; FS, forearm supination; AC, the average accuracy rate.

TABLE XI
CLASSIFICATION RESULTS OF AMPUTEES BY ANN

Subject	HC	HO	WE	WF	FP	FS	AC (%)
No. 1	88	36	100	24	88	100	72.67
No. 2	98	54	94	94	88	98	87.67

HC, hand closing; HO, hand opening; WE, wrist extension; WF, wrist flexion; FP, forearm pronation; FS, forearm supination; AC, average accuracy rate.

TABLE XII
COMPARISON BETWEEN THE PROPOSED METHOD AND PREVIOUS STUDIES ABOUT GESTURE RECOGNITION

Author	Number of electrodes	Number of hand movements	Classification method	Correct rate (%)	Reference
Ahmet	2	4	Discriminant analysis and SVM	96	[12]
Englehart	4	6	Linear Discriminant Analysis (LDA)	98	[14]
Khezri	4	6	Neuro–fuzzy inference system	92	[13]
Xing	4	7	SVM	98.39	[15]
Phinyomark	5	6	LDA	–	[16]
Delis	8	7	Linear discriminant analysis and ANN	–	[62]
Karimi	22	10	Genetic algorithm and ANN	98	[18]
Proposed method	3	6	WNN	94.67	This work

samples, and the test set also contains 300 samples. Due to the muscular atrophy of the amputees, the identification accuracy rates of hand motion commands are lower than those of normal subjects. However, the overall accuracy of WNN (85.17%) is still better than that of ANN (80.17%).

In this paper, we only used three sEMG sensors to achieve gesture recognition. Furthermore, in order to verify the contribution of our proposed sEMG pattern recognition system, we compared its results with previous studies, as listed in Table XII. Most researchers in these studies utilized more sEMG sensors to achieve the purpose of classifying more hand movements. As can be seen from Table XII, at least four electrodes are needed to classify six hand movements; however, we only need three sensors to realize the same number of hand motion commands. In practice, the user of a prosthetic hand will feel comfortable by using a small number of sEMG sensors. Therefore, the findings of this study offer significant advantages in application. Furthermore, the proposed method can be used in other industrial fields, such as the fault diagnosis [63]–[65] and the manipulator [66].

VI. CONCLUSION

In this paper, we have introduced a novel method to recognize six hand movements based on three sEMG sensors. We used DWT to extract the feature vector in the time-frequency domain; then, we used the proposed WNN classification system to identify the proposed six hand movements. It exhibited comparatively excellent results, in which the acquired overall accuracy was registered at 94.67% with a maximum accuracy rate of 100%. Moreover, as can be seen from the misclassification error and the omission error, the performance of WNN is better than that of ANN. In this paper, the proposed novel method can be effectively utilized in the pattern recognition of complex hand movements with only three sEMG sensors. Based on the above advantages, this method will be ultimately used for myoelectric prosthetic hand. In addition, the proposed method not only adapts to the amputees but also can be used to improve the motion control effects in the industrial field.

ACKNOWLEDGMENT

The authors would like to extend their sincere thanks to the Reviewers, the Associate Editor, and the Editor for their constructive suggestions and comments that improve the quality of the paper greatly. In addition, they also express their thanks to the subjects and the amputees for their excellent cooperation during the experiments.

REFERENCES

[1] Y. Oonishi, S. Oh, and Y. Hori, "A new control method for power-assisted wheelchair based on the surface myoelectric signal," *IEEE Trans. Ind. Electron.*, vol. 57, no. 9, pp. 3191–3196, Sep. 2010.
[2] J. Giho and Y. Choi, "EMG-based continuous control method for electric wheelchair," in *Proc. IEEE/RSJ Int. Conf. Intell. Robots Syst.*, 2014, pp. 3549–3554.
[3] J. F. Veneman, R. Kruidhof, E. E. G. Hekman, R. Ekkelenkamp, E. H. F. Van Asseldonk, and H. Van Der Kooij, "Design and evaluation of the LOPES exoskeleton robot for interactive gait rehabilitation," *IEEE Trans. Neural Syst. Rehabil. Eng.*, vol. 15, no. 3, pp. 379–386, Sep. 2007.
[4] K. Kiguchi and Y. Hayashi, "An EMG-based control for an upper-limb power-assist exoskeleton robot," *IEEE Trans. Syst. Man Cybern. B, Cybern.*, vol. 42, no. 4, pp. 1064–1071, Aug. 2012.
[5] M. Hennessey. (2014). *Clearpath Robotics Drives Robot with Arm Motions* [Online]. Available: http://www.clearpathrobotics.com/press_release/drive-robot-with-arm-motion/
[6] T. Kamali, R. Boostani, and H. Parsaei, "A multi-classifier approach to MUAP classification for diagnosis of neuromuscular disorders," *IEEE Trans. Neural Syst. Rehabil. Eng.*, vol. 22, no. 1, pp. 191–200, Jan. 2014.
[7] S. S. Nair, R. M. French, D. Laroche, and E. Thomas, "The application of machine learning algorithms to the analysis of electromyographic patterns from arthritic patients," *IEEE Trans. Neural Syst. Rehabil. Eng.*, vol. 18, no. 2, pp. 174–184, Apr. 2010.
[8] OttoBock. (2015). *SensorHand* [Online]. Available: http://professionals.ottobock.ca/cps/rde/xchg/ob_com_en/hs.xsl/3652.html
[9] Motion Control Inc. (2015). *Motion Control Hand* [Online]. Available: http://www.utaharm.com
[10] Bebionic3. (2015). *Bebionic3 Hand* [Online]. Available: http://bebionic.com/the_hand
[11] Medgadget. (2011). *Touch Bionics Introduces i-Limb Ultra Prosthetic Hand* [Online]. Available: http://www.medgadget.com/2011/09/touch-bionics-introduces-i-limb-ultra-prosthetic-hand.html
[12] A. Alkan and M. Günay, "Identification of EMG signals using discriminant analysis and SVM classifier," *Expert Syst. Appl.*, vol. 39, no. 1, pp. 44–47, Jan. 2012.
[13] M. Khezri and M. Jahed, "A neuro–fuzzy inference system for sEMG-based identification of hand motion commands," *IEEE Trans. Ind. Electron.*, vol. 58, no. 5, pp. 1952–1960, May 2011.
[14] K. Englehart, B. Hudgin, and P. A. Parker, "A wavelet-based continuous classification scheme for multifunction myoelectric control," *IEEE Trans. Biomed. Eng.*, vol. 48, no. 3, pp. 302–311, Mar. 2001.
[15] K. Xing, P. Yang, J. Huang, Y. Wang, and Q. Zhu, "A real-time EMG pattern recognition method for virtual myoelectric hand control," *Neurocomputing*, vol. 136, pp. 345–355, Jul. 2014.
[16] A. Phinyomark, P. Phukpattaranont, and C. Limsakul, "Feature reduction and selection for EMG signal classification," *Expert Syst. Appl.*, vol. 39, no. 8, pp. 7420–7431, Jun. 2012.
[17] J. Rafiee, M. A. Rafiee, F. Yavari, and M. P. Schoen, "Feature extraction of forearm EMG signals for prosthetics," *Expert Syst. Appl.*, vol. 38, no. 4, pp. 4058–4067, Apr. 2011.
[18] M. Karimi, H. Pourghassem, and G. Shahgholian, "A novel prosthetic hand control approach based on genetic algorithm and wavelet transform features," in *IEEE 7th Int. Colloq. Signal Process. Appl.*, 2011, pp. 287–292.

[19] A. Sappat, K. Mahaphonchaikul, M. Sangworasil, C. Pintavirooj, and A. Tuantranont, "Real-time identification of electromyographic signals from hand movement," in *Proc. IEEE 9th Int. Conf. Elect. Eng./Electron. Comput. Telecommun. Inf. Technol.*, 2012, pp. 1–4.

[20] L. Liu, P. Liu, E. A. Clancy, E. Scheme, and K. B. Englehart, "Electromyogram whitening for improved classification accuracy in upper limb prosthesis control," *IEEE Trans. Neural Syst. Rehabil. Eng.*, vol. 21, no. 5, pp. 767–774, Sep. 2013.

[21] A. H. Al-Timemy, G. Bugmann, J. Escudero, and N. Outram, "Classification of finger movements for the dexterous hand prosthesis control with surface electromyography," *IEEE J. Biomed. Health Informat.*, vol. 17, no. 3, pp. 608–618, May 2013.

[22] R. N. Khushaba, M. Takruri, J. V. Miro, and S. Kodagoda, "Towards limb position invariant myoelectric pattern recognition using time-dependent spectral features," *Neural Netw.*, vol. 55, pp. 42–58, Jul. 2014.

[23] D. Zhang, A. Xiong, X. Zhao, and J. Han, "PCA and LDA for EMG-based control of bionic mechanical hand," in *Proc. 2012 IEEE Int. Conf. Inf. Autom.*, 2012, pp. 960–965.

[24] A. Phinyomark, F. Quaine, S. Charbonnier, C. Serviere, F. Tarpin-Bernard, and Y. Laurillau, "EMG feature evaluation for improving myoelectric pattern recognition robustness," *Expert Syst. Appl.*, vol. 40, no. 12, pp. 4832–4840, Mar. 2013.

[25] H. Azami, H. Hassanpour, J. Escudero, and S. Sanei, "An intelligent approach for variable size segmentation of non-stationary signals," *J. Adv. Res.*, vol. 6, no. 5, pp. 687–698, Sep. 2015.

[26] G. Ercan and S. Abdulhamit, "Comparison of decision tree algorithms for EMG signal classification using DWT," *Biomed. Signal Process. Control*, vol. 18, pp. 138–144, Apr. 2015.

[27] G. Pfeiffer, "The diagnostic power of motor unit potential analysis: An objective Bayesian approach," *Muscle Nerve*, vol. 22, no. 5, pp. 584–591, Apr. 1999.

[28] G. Pfeiffer, "Sequential diagnostic decisions in quantitative motor-unit-potential analysis: A Bayesian approach," *Electroencephalogr. Clin. Neurophysiol.*, vol. 99, no. 4, p. 306, Oct. 1996.

[29] G. Pfeiffer and K. Kunze, "Discriminant classification of motor unit potentials (MUPs) successfully separate neurogenic and myopathic conditions," *Electroencephalogr. Clin. Neurophysiol.*, vol. 97, no. 5, pp. 191–207, Oct. 1995.

[30] Z. Barutcuoglu and C. DeCoro, "Hierarchical shape classification using Bayesian aggregation," in *Proc. IEEE Int. Conf. Shape Model. Appl.*, 2006, p. 44.

[31] Y. Xiang, B. Pant, A. Eisen, M. P. Beddoes, and D. Poole, "Multiply sectioned Bayesian networks for neuromuscular diagnosis," *Artif. Intell. Med.*, vol. 5, no. 4, pp. 293–314, Aug. 1993.

[32] A. Subasi, M. Yilmaz, and H. R. Ozcalik, "Classification of EMG signals using wavelet neural network," *J. Neurosci. Methods*, vol. 156, no. 1, pp. 360–367, Sep. 2006.

[33] D. M. Rittenhouse, H. A. Abdullah, R. J. Runciman, and O. Basir, "A neural network model for reconstructing EMG signals from eight shoulder muscles: Consequences for rehabilitation robotics and biofeedback," *J. Biomech.*, vol. 39, no. 10, pp. 1924–1932, Jul. 2006.

[34] S. Mefoued, "A second order sliding mode control and a neural network to drive a knee joint actuated orthosis," *Neurocomputing*, vol. 155, pp. 71–79, May 2015.

[35] E. W. Abel, P. C. Zacharia, A Forster, and T. L. Farrow, "Neural network analysis of the EMG interference pattern," *Med. Eng. Phys.*, vol. 18, no. 1, pp. 12–17, Jan. 1996.

[36] G. Cheron, A. M. Cebolla, A. Bengoetxea, F. Leurs, and B. Dan, "Recognition of the physiological actions of the triphasic EMG pattern by a dynamic recurrent neural network," *Neurosci. Lett.*, vol. 414, no. 2, pp. 192–196, Mar. 2007.

[37] C. I. Christodoulou and C. S. Pattichis, "Unsupervised pattern recognition for the classification of EMG signals," *IEEE Trans. Biomed. Eng.*, vol. 46, no. 2, pp. 169–178, Feb. 1999.

[38] J. U. Chu, I. Moon, and M. S. Mun, "A real-time EMG pattern recognition system based on linear-nonlinear feature projection for a multifunction myoelectric hand," *IEEE Trans. Biomed. Eng.*, vol. 53, no. 11, pp. 2232–2239, Nov. 2006.

[39] F. H. Chan, Y. S. Yang, F. K. Lam, Y. T. Zhang, and P. A. Parker, "Fuzzy EMG classification for prosthesis control," *IEEE Trans. Rehabil. Eng.*, vol. 8, no. 3, pp. 305–311, Sep. 2000.

[40] A. B. Ajiboye and R. F. Weir, "A heuristic fuzzy logic approach to EMG pattern recognition for multifunctional prosthesis control," *IEEE Trans. Neural Syst. Rehabil. Eng.*, vol. 13, no. 3, pp. 280–291, Sep. 2005.

[41] K. Momen, S. Krishnan, and T. Chau, "Real-time classification of forearm electromyographic signals corresponding to user-selected intentional movements for multifunction prosthesis control," *IEEE Trans. Neural Syst. Rehabil. Eng.*, vol. 15, no. 4, pp. 535–542, Dec. 2007.

[42] A. Subasi, "Classification of EMG signals using PSO optimized SVM for diagnosis of neuromuscular disorders," *Comput. Biol. Med.*, vol. 43, no. 5, pp. 576–586, Jun. 2013.

[43] F. Al Omari, J. Hui, C. Mei, and G. Liu, "Pattern recognition of eight hand motions using feature extraction of forearm EMG signal," *Proc. Natl. Acad. Sci. A, Phys. Sci.*, vol. 84, no. 3, pp. 473–480, Sep. 2014.

[44] M. A. Soltanmoradi, V. Azimirad, and M. Hajibabazadeh, "Detecting finger movement through classification of electromyography signals for use in control of robots," in *Proc. 2nd IEEE RSI/ISM Int. Conf. Robot. Mechatron.*, 2014, pp. 791–794.

[45] P. Geethanjali and K. K. Ray, "A low-cost real-time research platform for EMG pattern recognition-based prosthetic hand," *IEEE/ASME Trans. Mechatron.*, vol. 99, pp. 1–8, Oct. 2014.

[46] K. Kiguchi, T. Tanaka, and T. Fukuda, "Neuro-fuzzy control of a robotic exoskeleton with EMG signals," *IEEE Trans. Fuzzy Syst.*, vol. 12, no. 4, pp. 481–490, Aug. 2004.

[47] B. Azadbakht, K. Adinehvand, H. Zolata, O. Khayat, and H. C. Nejad, "An intelligent electromyogram signal characterization method based on neuro-fuzzy model," *J. Intell. Fuzzy Syst.*, vol. 27, no. 5, pp. 2623–2634, May 2014.

[48] S. A. Ahmad, M. A. Khalid, A. J. Ishak, M. Ali, and S. Hamid, "Surface EMG classification for prosthesis: Fuzzy logic vs. artificial neural network," in *Proc. Int. Conf. Bio-Inspired Syst. Signal Process.*, 2012, pp. 317–320.

[49] J. Yousefi and A. Hamilton-Wright, "Characterizing EMG data using machine-learning tools," *Comput. Biol. Med.*, vol. 51, pp. 1–13, Aug. 2014.

[50] R. H. Chowdhury, M. B. Reaz, M. A. B. M. Ali, A. A. Bakar, K. Chellappan, and T. G. Chang, "Surface electromyography signal processing and classification techniques," *Sensors*, vol. 13, no. 9, pp. 12431–12466, Sep. 2013.

[51] C. H. Kim and R. Aggarwal, "Wavelet transforms in power systems. I. General introduction to the wavelet transforms," *Power Eng. J.*, vol. 14, no. 2, pp. 81–87, Apr. 2000.

[52] X. Zhang, Y. Wang, and R. P. Han, "Wavelet transform theory and its application in EMG signal processing," in *Proc. 7th IEEE Int. Conf. Fuzzy Syst. Knowl. Discov.*, 2010, vol. 5, pp. 2234–2238.

[53] B. Cheng and G. Y. Liu, "Emotion recognition from surface EMG signal using wavelet transform and neural network," in *Proc. 2nd Int. Conf. Bioinformat. Biomed. Eng.*, 2008, pp. 1363–1366.

[54] S. G. Mallat, "A theory for multiresolution signal decomposition: the wavelet representation," *IEEE Trans. Pattern Anal. Mach. Intell.*, vol. 11, no. 7, pp. 674–693, Jul. 1989.

[55] S. G. Mallat, "Multifrequency channel decompositions of images and wavelet models," *IEEE Trans. Acoust. Speech Signal Process.*, vol. 37, no. 12, pp. 2091–2110, Dec. 1989.

[56] W. Dong, "Coiflet-type wavelets: Theory, design, and applications," Ph.D. dissertation, Dept. Elect. Comput. Eng., Univ. Texas, Austin, TX, USA, 1998.

[57] S. Kaur, G. Kaur, and D. Singh, "Comparative analysis of Haar and Coiflet wavelets using discrete wavelet transform in digital image compression," *Int. J. Eng. Res. Appl.*, vol. 3, no. 3, pp. 669–673, May 2013.

[58] R. Cheng and Y. Bai, "A novel approach to fuzzy wavelet neural network modeling and optimization," *Int. J. Electr. Power Energy Syst.*, vol. 64, pp. 671–678, Jan. 2015.

[59] S. Ganjefar and M. Tofighi, "Single-hidden-layer fuzzy recurrent wavelet neural network: Applications to function approximation and system identification," *Inf. Sci.*, vol. 294, pp. 269–285, Feb. 2015.

[60] M. R. Ahsan, M. I. Ibrahimy, and O. O. Khalifa, "The use of artificial neural network in the classification of EMG signals," in *Proc. 3rd FTRA Int. Conf. Mobile Ubiquitous Intell. Comput.*, 2012, pp. 225–229.

[61] S. A. Guvenc, M. Ulutas, and M. Demir, "Pattern recognition based analysis of arm EMG signals and classification with artificial neural networks," in *Proc. IEEE Signal Process. Commun. Appl. Conf.*, 2014, pp. 2209–2212.

[62] A. L. Delis, L. M. Revilla, D. D. Rodriguez, and A. R. Olaya, "On the use of surface EMG for recognizing forearm movements: Towards the control of an upper extremity exoskeleton," in *Proc. Andean Region Int. Conf.*, 2012, pp. 181–184.

[63] K. Hassen and A. Braham, "Recursive undecimated wavelet packet transform and DAG SVM for induction motor diagnosis," *IEEE Trans. Ind. Informat.*, vol. 11, no. 5, pp. 1059–1066, Oct. 2015.

[64] J. Neuzil, O. Kreibich, and R. Smid, "A distributed fault detection system based on IWSN for machine condition monitoring," *IEEE Trans. Ind. Informat.*, vol. 10, no. 2, pp. 1118–1123, May 2014.
[65] H. Henao *et al.*, "Trends in fault diagnosis for electrical machines: A review of diagnostic techniques," *IEEE Ind. Electron. Mag.*, vol. 8, no. 2, pp. 31–42, Jun. 2014.
[66] N. Nikdel, P. Nikdel, M. A. Badamchizadeh, and I. Hassanzadeh, "Using neural network model predictive control for controlling shape memory alloy-based manipulator," *IEEE Trans. Ind. Electron.*, vol. 61, no. 3, pp. 1394–1401, Mar. 2014.

Feng Duan received the B.E. and M.E. degrees in mechanical engineering from Tianjin University, Tianjin, China, in 2002 and 2004, respectively, and the M.S. and Ph.D. degrees in precision engineering from The University of Tokyo, Tokyo, Japan in 2006 and 2009, respectively.

Currently, he is an Associate Professor with Nankai University, Tianjin, China. His research interests include cellular manufacture systems, rehabilitation robots, and brain–machine interfaces.

Dr. Duan was the recipient of the Award of the Japanese Society for Artificial Intelligence (for the proposal of the standard platform in a home league 2014), the FANUC FA Robot Foundation Best Paper Award (2011), the Chinese Government Award for Outstanding Self-Financed Students Abroad (2008), the IEEE Conference on Automation Science and Engineering Best Student Paper Award (2008), a winner of RoboCup at Home Simulation in RoboCup Japan Open (Champion 2015), and a winner of RoboCup at Home Simulation in RoboCup Japan Open (First Runner-Up 2014).

Lili Dai received the B.E. degree in automation in 2014 from Nankai University, Tianjin, China, where she is currently working toward the Master's degree in automation in the College of Computer and Control Engineering.

Her research interests include pattern recognition and electromyogram-controlled prosthetic hands.

Wennan Chang received the B.E. degree in automation in 2014 from Nankai University, Tianjin, China, where he is currently working toward the Master's degree in automation in the College of Computer and Control Engineering.

His research interests include electromyogram signals and human gait analysis.

Zengqiang Chen received the B.S. degree in mathematics and the M.S. and Ph.D. degrees in automatic control from Nankai University, Tianjin, China, in 1987, 1990, and 1997, respectively.

Currently, he is a Professor with the Department of Automation, Nankai University. He has authored or coauthored over 100 journal papers. His research interests include intelligent optimizing control, intelligent computing, data mining, and image processing.

Chi Zhu (M'99) received the Ph.D. degree from The University of Tokyo, Tokyo, Japan, in 1999.

He was a Researcher with the National Institute for Resource and Environment and Yokohama National University in 1999 and 2000, respectively. He was a Postdoctoral Associate with the Massachusetts Institute of Technology, Cambridge, MA, USA, in 2001. He was an Associate Professor with the Maebashi Institute of Technology, Maebashi, Japan, from 2007 to 2015, where he is currently a Professor. His research interests include humanoid robots, walking-assisted robots, and power-assisted robots.

Wei Li (M'94) received the B.S. and M.S. degrees in electrical engineering from Northern Jiaotong University, Beijing, China, in 1982 and 1984, respectively, and the Ph.D. degree in electrical and computer engineering from the University of Saarland, Saarland, Germany, in 1991.

He was a Faculty Member with the Department of Computer Science and Technology, Tsinghua University, Beijing, China, from 1993 to 2001. From 1999 to 2001, he was a Research Scientist with the Department of Electrical Engineering, University of California, Riverside, CA, USA. Currently, he is a Professor with the Department of Computer Science, California State University, Bakersfield, CA, USA. His research interests include intelligent systems, robotics, fuzzy logic control and neural networks, multisensor fusion and integration, and graphical simulation.